14. Tiseo PJ, Perdomo CA, Friedhoff LT: Concurrent administration of donepezil HCl and ketoconazole: assessment of pharmacokinetic changes following single and multiple doses. *Br J Clin Pharmacol* 1998;46(Suppl. 1):30-34.

15. Galluzzi S, Zanetti O, Binetti G, Trabucchi M, Frisoni GB: Coma in a patient with Alzheimer's disease taking low dose trazodone and *Gingko biloba*. *J Neurol Neurosurg Psychiatry* 2000;68:679-680.

16. Otani K, Ishida M, Kaneko S, Mihara K, Ohkubo T, Osanai T, et al: Effects of carbamazepine coadministration on plasma concentrations of trazodone and its active metabolite, m-chlorophenylpiperazine. *Ther Drug Monit* 1996;18:164-167.

17. Durr D, Stieger B, Kullak-Ublick GA, Rentsch KM, Steinert HC, Meier PJ, et al: St John's wort induces intestinal P-glycoprotein/MDR1 and intestinal and hepatic CYP3A4. *Clin Pharmacol Ther* 2000;68:598-604.

18. Gurley BJ, Gardner SF, Hubbard MA, Williams DK, Gentry WB, Cui Y, et al: Cytochrome P450 phenotypic ratios for predicting herb-drug interactions in humans. *Clin Pharmacol Ther* 2002;72:276-287.

19. Shinozuka K, Umegaki K, Kubota Y, Tanaka N, Mizuno H, Yamauchi J, et al: Feeding of *Ginkgo biloba* extract (GBE) enhances gene expression of hepatic cytochrome P-450 and attenuates the hypotensive effect of nicardipine in rats. *Life Sci* 2002;70:2783-2792.

Steady-State Pharmacokinetics of a New Antipsychotic Agent Perospirone and Its Active Metabolite, and Its Relationship with Prolactin Response

Norio Yasui-Furukori, MD, PhD,† Hanako Furukori, MD, PhD,†‡ Taku Nakagami, MD,†§ Manabu Saito, MD,† Yoshimasa Inoue,‖ Sunao Kaneko, MD, PhD,† and Tomonori Tateishi, MD, PhD**

Abstract: The authors investigated steady-state pharmacokinetics of perospirone and its active metabolite hydroxyperospirone (ID-15036) and its prolactin response in 10 schizophrenic patients receiving 16 mg twice daily. Plasma concentrations of perospirone, hydroxyperospirone, and prolactin were monitored just before and up to 12 hours after the dosing. Thereafter, the dose was decreased to 8 mg twice daily in 8 patients, and drug concentrations were determined. The geometric means of peak concentration (C^{ss}_{max}), time to C^{ss}_{max} (t_{max}), area under the plasma concentration-time curve from 0 to 12 hours [AUC (0–12)], and elimination half-life at steady state were 8.8 ng/mL, 0.8 hours, 22.0 ng·h/mL, and 1.9 hours, respectively, for perospirone, and those of C^{ss}_{max}, t_{max}, and AUC (0–12) for hydroxyperospirone were 29.4 ng/mL, 1.1 hours, and 133.7 ng·h/mL, respectively. There were no differences in dose-normalized C^{ss}_{max} or AUC (0–12) perospirone and hydroxyperospirone between 16 mg/day and 32 mg/day of perospirone. Changes in prolactin concentration from 1 to 2 hours after the dosing were parallel with drug concentrations, and almost normal ranges of prolactin concentration were observed before the morning dose despite steady state. The current study indicated that perospirone is rapidly absorbed and rapidly eliminated, which influences the prolactin response. The active metabolite hydroxyperospirone may play an important role in the antipsychotic effect because the plasma concentration of this metabolite is higher than that of the parent compound.

Key Words: perospirone, hydroxyperospirone, plasma concentration, prolactin response, steady state

(*Ther Drug Monit* 2004;26:361–365)

Perospirone (*cis*-N-[4-[4-(1,2-benzisothiazol-3-yl)-1-piperazinyl]butyl]cyclohexane-1,2-dicarboximide) (Fig. 1) is a new serotonin 5-HT_2 and dopamine D_2 antagonist based on receptor binding experiments.[1,2] It has been reported that perospirone was effective against positive, negative, and general symptoms in patients with schizophrenia. Compared with haloperidol 2 to 12 mg/day, perospirone 8 to 48 mg/day was significantly more effective against negative symptoms and tended to be more effective against general symptoms and most positive symptoms in a trial in 145 patients with schizophrenia and is well tolerated compared with haloperidol treatment.[3] Based on these findings, perospirone has been marketed in the treatment of acute and chronic schizophrenic patients in Japan since 2001.

Preclinical in vitro studies with human liver microsomes and recombinantly expressed microsomes have suggested that perospirone undergoes hydroxylation, N-dealkylation, and S-oxidation, which are catalyzed by CYP1A1, 2C8, 2D6, and 3A4.[3,4] Contribution to perospirone metabolism is CYP3A4 >> CYP2D6 > CYP2C8 = CYP1A1. Of 17 metabolites of perospirone, only hydroxyperospirone (ID-15036), in which the cyclohexane-1,2-dicarboximide moiety is hydroxylated (Fig. 1), has pharmacologically active antiserotonergic effects, although it has one-eighth the activity of the parent compound based on receptor affinity studies (K_i 4.9 vs 0.61 nM) and animal behavioral studies (ED50 93 vs 11 μg/kg).[5] In addition, a phase 1 study using healthy volunteers showed that the plasma concentration of hydroxyperospirone is higher than that of perospirone after single or repeated oral doses of perospirone, although subclinical doses were used.[6] Therefore, it is clinically important for a pharmacokinetic and pharmacodynamic study to detect not only perospirone but also hydroxyperospirone in human plasma.

To our knowledge, however, there is no report of pharmacokinetic profile at steady state for these compounds. Recently, we developed a method for sensitive determination of perospirone and hydroxyperospirone applicable in pharmacokinetic studies.[7] Thus, we examined the dose-related pharmacokinetic profile at steady state of perospirone and hy-

Received for publication July 22, 2003; accepted May 5, 2004.

From the *Department of Clinical Pharmacology, Hirosaki University School of Medicine, Hirosaki, Japan; †Department of Neuropsychiatry, Hirosaki University School of Medicine, Hirosaki, Japan; ‡Department of Psychiatry, Kuroishi-Akebono Hospital, Kuroishi, Japan; §Department of Psychiatry, Hirosaki Aiseikai Hospital, Hirosaki, Japan; and ‖Pharmaceutical Technology Division, Mitsubishi Pharma, Fukuoka, Japan.

Address correspondence and reprint requests to Norio Yasui-Furukori, MD, PhD, Department of Clinical Pharmacology, Hirosaki University, School of Medicine, Hirosaki 036-8562, Japan (e-mail: yasufuru@cc.hirosaki-u.ac.jp).

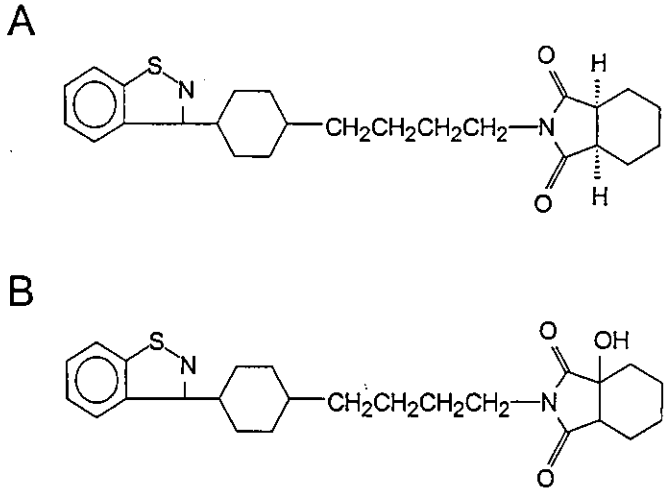

FIGURE 1. Chemical structure of perospirone (A) and hydroxyperospirone (ID-15036) (B).

droxyperospirone in schizophrenic patients receiving perospirone. In addition, we investigated the prolactin response to this drug.

MATERIALS AND METHODS

Subjects

The subjects consisted of 10 (3 male and 7 female) physically healthy inpatients who met the criteria for schizophrenia according to *Diagnostic and Statistical Manual of Mental Disorders, Version IV* criteria.[8] The median age (and range) was 47.0 (30–72) years, and that of body weight was 62.5 (42–96) kg. The study protocol was approved by the Ethics Committee of Hirosaki University School of Medicine, and all patients gave their written informed consent to participate in the study.

Protocol

The present study was performed independently of the company promoting perospirone on the market (Sumitomo Pharmaceutical, Osaka, Japan) except for the donation of pure compounds of perospirone and its major metabolite, hydroxyperospirone (ID-15036). All patients received 16 mg of perospirone (Lullan®; Sumitomo Pharmaceutical, Osaka, Japan) twice daily (8 AM, 8 PM) for at least 2 weeks. No other drugs were given except biperiden 4–6 mg in 2 patients, flunitrazepam 1–4 mg in 8 patients, and sennoside 12–48 mg in 5 patients. After an overnight fast, each patient took an oral 16-mg dose of perospirone with a cup of tap water at 8:00 AM. No food was allowed until 3 hours after the dosing. Blood samplings (10 mL each) were performed just before and at 0.5, 1, 2, 3, 4, 6, 8, and 12 hours after the dosing using a peripheral intravascular catheter (JELCO*Plus® IV catheter, Johnson & Johnson, Belgium). Thereafter, the dose was decreased to 8 mg twice a day in 8 patients based on their mental status. Blood samplings were performed at least 2 weeks after changing doses in the same manner as on the first sampling day. Other medications were fixed throughout the study period.

Assay

Plasma concentrations of perospirone and hydroxyperospirone were determined by the HPLC method developed in our laboratory.[7] The limits of quantifications were 0.3 ng/mL and intra- and interassay CV values were less than 5% at 0.3 ng/mL of both compounds.

Plasma prolactin concentrations were measured by enzyme immunoassay (IMX Prolactin Dinapack, Dainabot Ltd, Tokyo, Japan). The limit of detection of prolactin concentration was 1.0 ng/mL, and intra- and interassay CV values were less than 5.6% at plasma concentrations of 8.0, 20.0, and 40.0 ng/mL.

Data Analyses of Pharmacokinetics

The steady-state peak concentration $[(C^{ss})_{max}]$ and concentration peak time (t_{max}) were obtained directly from the original data. The area under the plasma concentration–time curve [AUC (0–12)] was calculated with use of the trapezoidal rule. The terminal rate constant (k_e) used for the extrapolation was determined by regression analysis of the log-linear part of the concentration–time curve for each subject. The elimination half-life was determined by $0.693/k_e$. Mean residence times (MRT) were calculated by AUMC/AUC, where AUMC is the area under the moment-versus-time curve and was calculated with use of the trapezoidal rule with time adjustment. Steady-state volume of distribution (V_{ss}) were calculated by (Dose × AUMC)/(AUC × AUC).

The paired *t*-test for the comparison of 16 mg/day versus 32 mg/day was conducted on pharmacokinetic parameters corrected by daily dosage. A P value of 0.05 or less was regarded as significant. SPSS 8.0.1 for Windows (SPSS Japan Inc, Tokyo) was used for these statistical analyses.

RESULTS

The pharmacokinetic parameters of perospirone and hydroxyperospirone in 10 schizophrenic patients receiving 32 mg daily are summarized in Table 1. Individual plasma concentrations of perospirone, hydroxyperospirone, and prolactin in 10 patients receiving 32 mg/day of perospirone are shown in Figure 2. There was large individual variability of plasma concentrations of perospirone (20-fold) and hydroxyperospirone (10-fold), respectively. However, 2 elderly female patients (68 and 72 years) with coadministration of flunitrazepam tended to have higher plasma drug concentration [AUC (0–12h) 95 ng·h/mL and 108 ng·h/mL], compared with mean corresponding value in other patients (19 ng·h/mL). There was no differ-

TABLE 1. Steady-State Pharmacokinetic Parameters of Perospirone, Hydroxyperospirone and Prolactin in 10 Schizophrenic Patients Receiving 32 mg/day of Perospirone

	Geometric Mean	Range
Perospirone		
$(C^{SS})_{max}$ (ng/mL)	8.8	2.2–43.9
t_{max} (h)	0.8	0.5–2.0
AUC (0–12) (ng · h/mL)	22.0	5.8–108
V_{SS} (L)	1733	356–5246
MRT (h)	1.2	0.9–1.6
$t_{1/2}$ (h)	1.9	0.8–3.3
Hydroxyperospirone		
$(C^{SS})_{max}$ (ng/mL)	29.4	13.4–130.9
t_{max} (h)	1.1	0.5–2.0
AUC (0–12) (ng · h/mL)	133.7	56–484
Prolactin*		
Males		
Predose concentration (ng/mL)	7.1	3.5–24.0
$(C^{SS})_{max}$ (ng/mL)	62.3	40.0–77.9
t_{max} (h)	1.6	1.0–2.0
AUC (0–12) (ng · h/mL)	189.5	128.2–406.3
Females		
Predose concentration (ng/mL)	9.0	3.0–45.4
$(C^{SS})_{max}$ (ng/mL)	150.9	51.3–210.0
t_{max} (h)	1.2	1.0–2.0
AUC (0–12) (ng · h/mL)	424.7	113.3–1170.0

*Normal range: 2–15 ng/mL.

ence in pharmacokinetic parameters between results with and without coadministration of flunitrazepam.

There were no differences in dose-normalized peak concentration $[(C^{ss})_{max}]$ or AUC (0–12) of perospirone and hydroxyperospirone between 16 mg/day and 32 mg/day of perospirone.

Although almost normal ranges of prolactin concentration (2–15 ng/mL)[9] were observed before the morning dose despite steady state, plasma prolactin concentration increased after the dosing. Hysteresis plots of prolactin concentration versus perospirone concentration showed counterclockwise rotation but linearity from 1 or 2 to 12 hours after the dosing in both male and female patients (Fig. 3). These findings indicate that the prolactin response lags behind the drug concentrations, but prolactin concentration decreased with perospirone concentration. The geometric mean of $(C^{ss})_{max}$ or AUC prolactin concentration during the perospirone treatment in female patients was greater than that in male patients $[(C^{ss})_{max}$ 150.9 vs 62.3 ng/mL, AUC (0–12) 424.7 vs 189.5 ng·h/mL], although there was no significant difference because of the small number of male subjects.

DISCUSSION

Perospirone was rapidly absorbed (t_{max} = 0.8 hour) compared with such other neuroleptics as haloperidol (1.7 hours),[10] chlorpromazine (1–4 hours),[11] and zotepine (3.8 hours)[12] and was also rapidly eliminated ($t_{½}$ = 1.9 hours). This pharmacokinetic profile suggests that perospirone has early onset including sedative effects and early disappearance of its efficacy when it is initiated and discontinued, although there are no specific data about the receptor binding time of perospirone and active metabolite(s) to date.

In the present study, steady-state plasma concentration of hydroxyperospirone was higher than that of perospirone, which is in line with a previous phase 1 study. The results of this study showed that exposure to hydroxyperospirone was approximately 6-fold greater than that of perospirone. Hy-

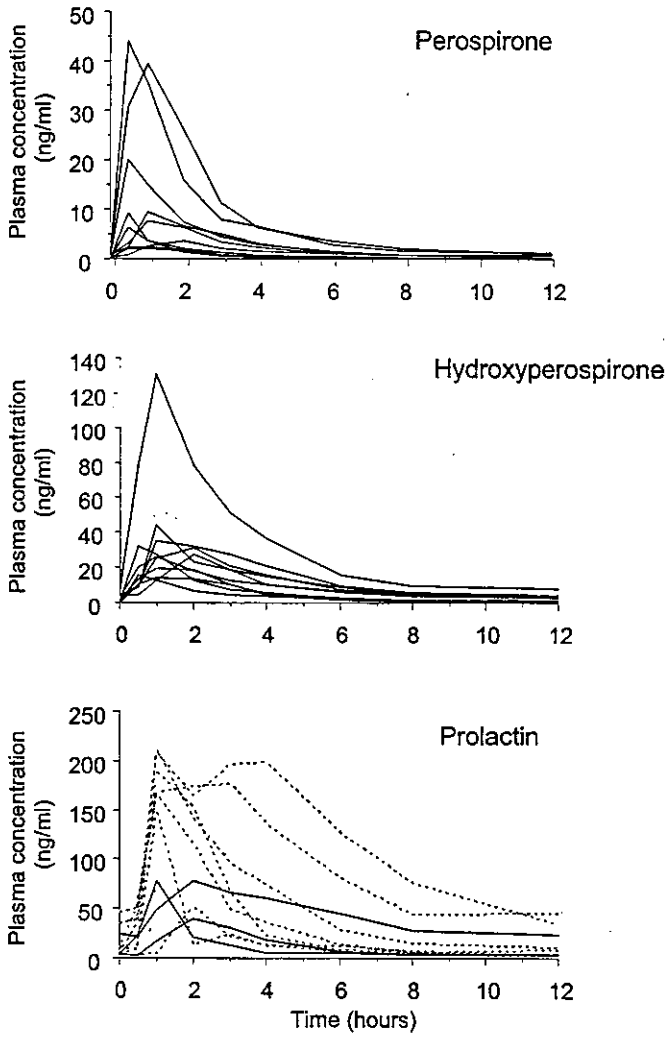

FIGURE 2. Interindividual plasma concentration–time curves for perospirone (top), hydroxyperospirone (ID-15036) (middle), and prolactin (bottom). For prolactin, solid lines represent male and dotted lines represent female patients.

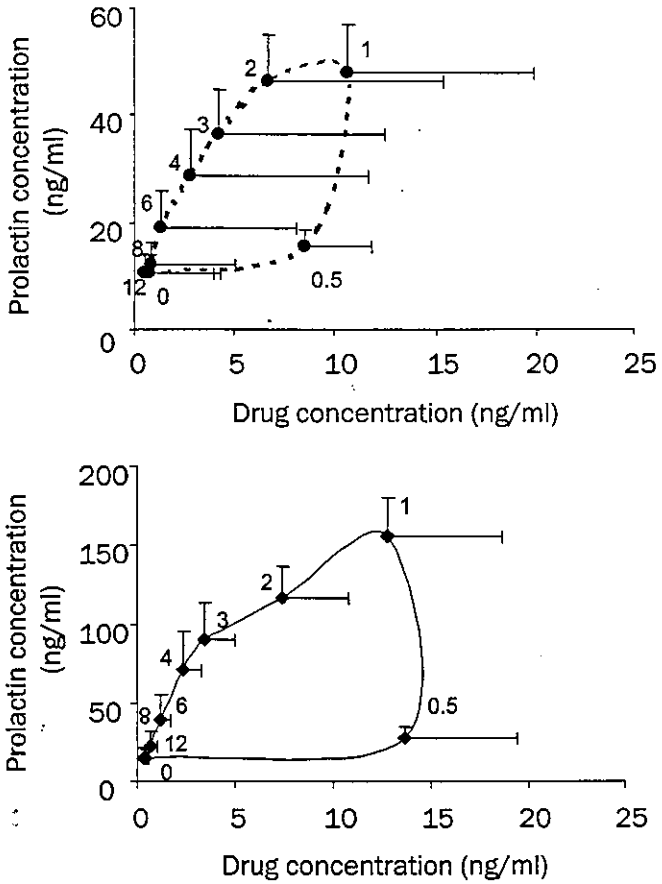

FIGURE 3. Hysteresis plots of mean prolactin concentration versus mean perospirone concentration in 3 male (top) and 7 female patients (bottom) following a 16-mg dose of perospirone at steady state with repeated 16-mg doses twice daily. Time of samplings is indicated. Horizontal and vertical error bars indicate standard errors for perospirone and prolactin, respectively.

droxyperospirone has a pharmacologically active antiserotonergic property, although it has one-eighth the activity of its parent compound.[5] Thus, because of the greater plasma concentration and pharmacodynamic potency between perospirone and hydroxyperospirone, hydroxyperospirone may play an important role in atypical antipsychotic effect.

There was large interindividual variability in plasma levels of perospirone (20-fold) and hydroxyperospirone (10-fold) despite similar doses. Thus, careful therapeutic drug monitoring (TDM) of these compounds is recommended for individualized medication control. However, 4 out of 10 patients had undetectable concentrations of perospirone just before the dosing. Also, with the exception of an elderly patient, 5 other patients had very low drug concentrations (less than 1.0 ng/mL). These findings suggest that accumulation of perospirone at steady state is unlikely to occur at least up to 32 mg/day, and trough concentration of perospirone $[(C^{ss})_{min}]$ may not be suitable for TDM. Therefore, routine sampling time should be changed from just before the dosing to a new sampling time (eg, 4–6 hours after dosing). When individual optimal dosage is calculated using TDM data, blood samplings at several time points may be considered.

Two elderly female patients had a much higher plasma drug concentration than other patients. These 2 patients were concomitantly administered flunitrazepam. However, it is unlikely that flunitrazepam has an inhibitory or inducing effect on disposition of perospirone or hydroxyperospirone because there was no difference between levels with and without flunitrazepam coadministration. Thus, a further study is necessary to confirm the effect of aging on pharmacokinetics or pharmacodynamics of perospirone in a large number of subjects.

No differences in dose-normalized drug concentrations have been observed for perospirone and hydroxyperospirone. We have several plausible explanations. In vitro studies showed that CYP3A4 is responsible for the major metabolic pathway from perospirone to hydroxyperospirone.[3] It is known that CYP3A4 is a high-capacity enzyme, and the largest amount is in human liver.[14] In addition, preliminary animal studies determined at least 10 metabolites of perospirone, indicating that perospirone should have several alternative metabolic pathways.

Only perospirone but not hydroxyperospirone has antidopaminergic activity. The elevation of prolactin concentration after taking neuroleptics is associated with an antagonistic effect on the dopamine D2 receptor.[14,15] A clinical study[17] has suggested that prolactin levels in schizophrenic patients determined 10–14 hours after perospirone dosing are within normal range (2–15 ng/mL).[9] Likewise, prolactin concentrations before the morning dose were almost in the normal range in this study, although prolactin concentrations were elevated with a delay after the morning dose but decreased with elimination of perospirone from plasma. Therefore, these findings imply that blood sampling before the administration underestimate perospirone-related hyperprolactinemia. Blood samplings at several time points or a few hours after the morning dose are recommended when there are adverse effects related to hyperprolactinemia.

In conclusion, perospirone is rapidly absorbed and rapidly eliminated, thereby influencing prolactin response. Plasma concentrations of perospirone and its active metabolite hydroxyperospirone increased proportionately with doses. The hydroxyperospirone may play an important role in the antipsychotic effect because the plasma concentration of this active metabolite is higher than that of the parent compound.

ACKNOWLEDGMENT

This study was supported by a grant from Hirosaki Research Institute for Neurosciences.

REFERENCES

1. Kato T, Hirose A, Ohno Y, et al. Binding profile of SM-9018, a novel antipsychotic candidate. *Jpn J Pharmacol.* 1990;54:478–481.
2. Schotte A, Bonaventure P, Janssen PF, et al. In vitro receptor binding and in vivo receptor occupancy in rat and guinea pig brain: risperidone compared with antipsychotics hitherto used. *Jpn J Pharmacol.* 1995;69:399–412.
3. Onrust SV, McClellan K. Perospirone. *CNS Drugs.* 2001;15:329–337.
4. Mizuno Y, Tani N, Komuro S, et al. In vitro metabolism of perospirone in rat, monkey and human liver microsomes. *Eur J Drug Metab Pharmacokinet.* 2003;28:59–66.
5. Ishibashi T, Ohno Y, Tokuda K, et al. CNS pharmacological actions of the major metabolites of perospirone hydrochloride. *Kiso to Rinsyo.* 1997;31: 893–902. (In Japanese)
6. Inanaga K, Irie N, Urae A, et al. Phase I study of perospirone HCl (SM-9018). *Kiso to Rinsyo.* 1997;31:2113–2157. (In Japanese)
7. Yasui-Furukori N, Inoue Y, Tateishi T. Determination of a new atypical antipsychotic agent perospirone and its metabolite in human plasma by automated column-switching high-performance liquid chromatography. *J Chromatgr B.* 2003;789:239–245.
8. The American Psychiatric Association. *Diagnostic and Statistical Manual for Mental Disorders, 4th ed.* Washington, DC: The American Psychiatric Association, 1994.
9. Fauci AS, Braunwald E, Isselbacher KJ, et al. *Harrison's Principles of Internal Medicine, 14th ed.* New York; McGraw-Hill, 1998.
10. Froemming JS, Lam YW, Jann MW, et al. Pharmacokinetics of haloperidol. *Clin Pharmacokinet.* 1989;17:396–423.
11. Dahl SG, Strandjord RE. Pharmacokinetics of chlorpromazine after single and chronic dosage. *Clin Pharmacol Ther.* 1977;21:437–448.
12. Tanaka O, Kondo T, Otani K, et al. Single oral dose kinetics of zotepine and its relationship to prolactin response and side effects. *Ther Drug Monit.* 1998;20:117–119.
13. Rowland M, Tozer TN. eds. *Clinical Pharmacokinetics; Concepts and Applications, 3rd ed.* Baltimore: Williams & Wilkins, 1995:230–247.
14. Watkins PB. Noninvasive tests of CYP3A enzymes. *Pharmacogenetics.* 1994;4:171–184.
15. Kapur S, Roy P, Daskalakis J, et al. Increased dopamine d(2) receptor occupancy and elevated prolactin level associated with addition of haloperidol to clozapine. *Am J Psychiatry.* 2001;158:311–314.
16. Hamner M. The effects of atypical antipsychotics on serum prolactin levels. *Ann Clin Psychiatry.* 2002;14:163–173.
17. Togo T, Iseki E, Shoji M, et al. Prolactin levels in schizophrenic patients receiving perospirone in comparison to risperidone. *J Pharmacol Sci.* 2003;91:259–262.

Effect of localization of missense mutations in *SCN1A* on epilepsy phenotype severity

K. Kanai, MD; S. Hirose, MD; H. Oguni, MD; G. Fukuma, MD; Y. Shirasaka, MD; T. Miyajima, MD; K. Wada, MD; H. Iwasa, MD; S. Yasumoto, MD; M. Matsuo, MD; M. Ito, MD; A. Mitsudome, MD; and S. Kaneko, MD

Abstract—*Background and Methods:* Many missense mutations in the voltage-gated sodium channel subunit gene *SCN1A* were identified in patients with generalized epilepsy with febrile seizures plus (GEFS+) and severe myoclonic epilepsy of infancy (SMEI), although GEFS+ is distinct from SMEI in terms of clinical symptoms, severity, prognosis, and responses to antiepileptic drugs. The authors analyzed the localization of missense mutations in *SCN1A* identified in patients with GEFS+ and SMEI to clarify the phenotype-genotype relationships. *Results:* Mutations in SMEI occurred more frequently in the "pore" regions of *SCN1A* than did those in GEFS+. These SMEI mutations in the "pore" regions were more strongly associated than mutations in other regions with the presence of ataxia and tendency to early onset of disease. The possibility of participation of ion selectivity dysfunction of the channel in the pathogenesis of SMEI was suggested by a mutation in the pore region (R946C) identified in a SMEI patient. *Conclusions:* There was a significant phenotype-genotype relationship in generalized epilepsy with febrile seizures plus and severe myoclonic epilepsy of infancy with *SCN1A* missense mutations. More severe sodium channel dysfunctions including abnormal ion selectivity that are caused by mutations in the pore regions may be involved in the pathogenesis of SMEI.

NEUROLOGY 2004;63:329–334

Mutations in several ion channel genes associated with some epileptic syndromes have recently been reported.[1] In *SCN1A*, the neuronal voltage-gated sodium channel α1-subunit gene, missense mutations first were identified in patients with generalized epilepsy with febrile seizures plus (GEFS+ [MIM 604236]),[2] an autosomal dominant epilepsy characterized by febrile seizures in children (often persisting beyond 6 years of age) and afebrile seizures in adults. Since then, several patients or families of GEFS+ with *SCN1A* mutations have been reported.[3-9]

De novo mutations of *SCN1A* also have been identified in patients with severe myoclonic epilepsy of infancy (SMEI).[10] SMEI is a rare disorder, characterized by various types of generalized and partial seizures (including myoclonic ones) initially induced by fever, as well as by delayed psychomotor development after the second year of life, and refractoriness to drug therapy.[1]

To date, many kinds of *SCN1A* mutations have been reported in SMEI patients.[7-15] Moreover, *SCN1A* mutations have been identified in patients who do not fulfill all the SMEI criteria (borderline SMEI [SMEB][12,14,16]) and in those with intractable childhood epilepsies with frequent generalized tonic-clonic seizures [ICEGTC][7]).

Truncation mutations generally cause a more severe disturbance of protein functions than do missense mutations, almost all the reported truncation mutations of *SCN1A* having resulted in the phenotype SMEI, SMEB, or ICEGTC. Missense mutations initially were identified in patients with GEFS+ but later in patients with SMEI, SMEB, and ICEGTC.[7-9,12-15] GEFS+ is distinct from SMEI in terms of its clinical symptoms, severity, prognosis, and responses to antiepileptic drugs. Why do similar missense mutations in *SCN1A* cause two such different phenotypes (GEFS+/SMEI)? Analysis of the phenotype-genotype relationship in GEFS+ and SMEI patients with *SCN1A* missense mutations will provide understanding of the mechanisms of pathogenesis of those phenotypes, and perhaps ultimately of epilepsy.

We carried out a meta-analysis of the missense

From the Department of Neuropsychiatry (Drs. Kanai, Iwasa, and Kaneko), Hirosaki University School of Medicine, Aomori; Department of Pediatrics (Drs. Hirose, Fukuma, Yasumoto, and Mitsudome), Fukuoka University; Department of Pediatrics (Dr. Oguni), Tokyo Women's Medical University; Kobe City General Hospital (Dr. Shirasaka); Department of Pediatrics (Dr. Miyajima), Tokyo Medical University; Department of Occupational Therapy (Dr. Wada), School of Health Science, Hirosaki University; Department of Pediatrics (Dr. Matsuo), Saga Medical School; Department of Pediatrics (Dr. Ito), Shiga Medical Center for Children; and Department of Neurology (Dr. Kanai), Chiba University School of Medicine, Japan.

Supported in part by a grant for Epilepsy from the Ministry of Health and Welfare of Japan. The research was conducted as part of a comprehensive project organized by The Epilepsy Genetic Study Group, Japan (Chairperson, Sunao Kaneko), and supported in part by Grants-in-Aid for Scientific Research from the Ministry of Education, Culture, Sports, Science and Technology of Japan (09570206, 13035049, 12470174, 12559010, 14658263); the Epilepsy Research Foundation; the Uehara Memorial Foundation; and the Hirosaki Research Institute for Neuroscience.

Received September 17, 2003. Accepted in final form March 18, 2004.

Address correspondence and reprint requests to Dr. Kazuaki Kanai, Department of Neuropsychiatry, Hirosaki University School of Medicine, 5 Zaifu-cho, Hirosaki, Aomori 036–8562, Japan; e-mail: VZR03355@nifty.ne.jp

Table 1 Summary of clinical information on SMEI/SMEB patients

Patient	Mutation	Sex	Myoclonic seizures	Atypical absence	Onset, mo	Family history	Ataxia	Mental Retardation	Phenotype	Segment	Ref.
1	E78D								SMEI	N-terminal	8
2	R101Q	M	−	−	6	+		Moderate	SMEB	N-terminal	14
3	S103G	F	+	−	3	+	+	Severe	SMEI	N-terminal	7
4	T112I	F	+	+	7	−	+	Severe	SMEI	N-terminal	7
5	G177E								SMEI	S2–S3 linker	8
6	W190R	F	−	+	7	−		Moderate	SMEI	S3	14
7	I227S								SMEI	S4	8
8	I227S								SMEI	S4	8
9	I227S								SMEI	S4	8
10	G265W	M	+	−	5	+	−	Mild	SMEI	S5	7
11	W280R								SMEI	S5–S6 linker	8
12	T297I	F							SMEI	S5–S6 linker	8
13	G343E	M	−	+	4	−	+	Severe	SMEI	S5–S6 linker	7
14	R393H		+	+	6	+	+	Severe	SMEI	S5–S6 linker	13
15	Y426N								SMEI	I–II linker	8
16	T808S/N1011I	M	−	−	9	−	−	Moderate	SMEB	S2	7
17	F901C	M	−	−	5	−	−		SMEB	S5	12, 16
18	R931C	M	+	−	5	−	+		SMEI	S5–S6 linker	12, 16
19	R931C	F	−	−	6	−	+		SMEB	S5–S6 linker	12, 16
20	M934I	F	+	+	6	−		Moderate	SMEI	S5–S6 linker	14
21	M934I	F	−	−	7	+		Mild	SMEB	S5–S6 linker	14
22	H939Q		−	−	4.5	−	+	Moderate	SMEB	S5–S6 linker	13
23	V944A	F	−	−	5	−		Moderate	SMEB	S5–S6 linker	14
24	R946C	F	+	−	6	+		Moderate	SMEI	S5–S6 linker	14
25	R946C	M	−	−	4	−		Severe	SMEB	S5–S6 linker	14
26	R946H	F	−	−	4	+		Severe	SMEB	S5–S6 linker	14
27	C959R		+	+	3	−	+	Severe	SMEI	S5–S6 linker	13
28	M960V	F	+	+	6	+	−	Severe	SMEI	S5–S6 linker	7
29	G979R	M	−	−	4	+	−	Severe	SMEB	S6	7
30	V983A	M	−	−	3	+	+	Severe	SMEB	S6	7
31	N985I	F	+	−	4	−	−	Severe	SMEI	S6	7

Blank = data not available; SMEI = severe myoclonic epilepsy of infancy; SMEB = borderline SMEI.

mutations of *SCN1A* identified in patients with GEFS+, SMEI, and SMEI-related disorders (SMEB and ICEGTC) to clarify the phenotype-genotype relationships in GEFS+ and SMEI patients.

Subjects and methods. *Subjects.* Up to now, 68 missense *SCN1A* mutations have been reported in patients with GEFS+, SMEI, and SMEB and ICEGTC. Of these, 12 were reported by our group,[5,14] 56 by others.[2-4,6-10,12-14]

We re-analyzed the phenotypes of all the patients reported and classified them into three categories: core SMEI (SMEI), borderline SMEI (SMEB), and GEFS+. All those reported who fulfilled the diagnostic criteria of the International League against Epilepsy (ILAE)[17] were classified in the SMEI category. We defined patients with SMEB as those who met most of the ILAE diagnostic criteria but did not show both myoclonic and atypical absence seizures. We re-analyzed all the cases of patients with borderline SMEI[12,14,16] and ICEGTC,[7] and classified all but one (V1611F) in the SMEB category. We considered that the ICEGTC patient with V1611F[7] should be included in the GEFS+ spectrum, because of the absence of myoclonic/atypical absence seizure, mental retardation, ataxia, and brain atrophy.

In 13 reports,[2-10,12-15] 42 missense mutations were identified in 45 patients with SMEI, 18 in 17 patients with SMEB, and 14 in those with GEFS+ (tables 1 and 2). Two mutations (T808S and N1011I) were identified in one SMEB patient.[7] Three mutations (R931C, M934I, and R946C) were identified in both those with SMEI and SMEB,[12,14,16] two mutations (P1668A and M1852T) each in SMEI and GEFS+,[9,14] and one mutation (T1709I) in SMEB and GEFS+.[7]

The following clinical data on SMEI and SMEB patients were reported: patients' sex (n = 42),[7,10,12,14-16] disease onset (n = 48),[7,10,12-16] evaluation of mental retardation (slight, moderate, severe; n = 38),[7,10,13-15] and presence of ataxia (n = 35).[7,10,12-14,16]

To define the functional difference in the positions of mutations in the *SCN1A* amino acid sequence, we used the database SWISSPROT for the amino acid sequence of *SCN1A* and its predicted structure (SWISSPROT accession number P35498).

We defined the S5, S5-S6 linker, and S6 segments of internal homologous domains as the "pore" region; the S4 segment as the "voltage sensor" region; region in the four internal homologous

Table 1 Continued

Patient	Mutation	Sex	Myoclonic seizures	Atypical absence	Onset, mo	Family history	Ataxia	Mental Retardation	Phenotype	Segment	Ref.
32	L986F	F	+	+	4	−	+	Moderate	SMEI	S6	10
33	S1231R	M	+	−	7	−	−	Moderate	SMEI	S1	7
34	G1233R								SMEI	S1	8
35	F1263L	F	+	+	10	+	−	Severe	SMEI	S2	7
36	L1265P	F	+	−	6	−	+		SMEI	S2	12, 16
37	A1326P	M	+	−	6	+	−	Moderate	SMEI	S4	15
38	L1355P	F	−	−	10	−		Moderate	SMEB	S5	14
39	V1390M	F			7	−			SMEI	S5–S6 linker	12
40	W1434R	F	+	−	4	−	+		SMEI	S5–S6 linker	12, 16
41	W1434R		+	+	2.5	−	+	Moderate	SMEI	S5–S6 linker	13
42	Q1450R	M	−	−	8	−	+		SMEB	S5–S6 linker	12, 16
43	L1461I								SMEI	S6	8
44	F1463S								SMEI	S6	8
45	P1632S	M	−	−	3	−	−	Severe	SMEB	S3–S4	7
46	R1648R	F	+	−	3	+	+		SMEI	S4	12, 16
47	F1661S		+	−	9	−	−	severe	SMEI	S4–S5	13
48	P1668A	F							SME1	S4–S5	8
49	G1674R	F	−	−	5	−	+		SMEB	S5	12,16
50	A1685D	M	+	−	6	+	+	Severe	SMEI	S5	7
51	F1692S	F	+	−	13	−		Severe	SMEI	S5	14
52	Y1694C	F	+	+	6	+		Severe	SMEI	S5	14
53	T1709I	M	−	−	9	+	+	Moderate	SMEB	S5–S6 linker	7
54	G1749E		+	+	8	+	+	Moderate	SMEI	S5–S6 linker	13
55	M1780T								SMEI	S6	8
56	Y1781C	M	−	+	10	+		Mild	SMEI	S6	14
57	F1808L	F	−	−	11	−	+	Moderate	SMEB	C-terminal	7
58	W1812G	M	+	−	5	−	+	Severe	SMEI	C-terminal	7
59	F1831S	F	+	+	8	−	+	Severe	SMEI	C-terminal	7
60	M1852T								SMEI	C-terminal	9
61	E1881D	M	+	+	6	+	−	Severe	SMEI	C-terminal	15
62	T1909I	F	+	+	7	−	−		SMEI	C-terminal	12, 16

domains except "pore" regions as "other homologous domain" region; region in the four internal homologous domains except S5-S6 ("pore") and S4 ("voltage sensor") segments as the "insulating" region[18]; and the regions except the four internal homologous domains as "regions except the homologous domains."

Statistical analysis. Statistical analyses of the distribution patterns of the missense mutations in *SCN1A* and evaluations of mental retardation in the patient groups in the GEFS+, SMEI, SMEB, and total SMEI groups were made with the χ^2 test on two independent samples with SPSS software (SPSS Japan Inc.). Fisher's exact test was used for the statistical analyses of the distribution of missense mutations within the four homologous domains in *SCN1A*, sex, and the presence of ataxia in these groups. Differences in the medians of disease onset in the groups were compared by the Mann-Whitney *U* test. All statistical tests were two-sided.

Results. Figure 1A, table 1, and table 2 show the localization of missense mutations in *SCN1A*. Many that caused SMEI and SMEB occurred in the S5, S5-S6 linker, and S6 segments, considered the "pore" forming region in sodium channels (see table 2). When the regions in *SCN1A* were arranged into three groups, "pore" region, "other homologous domain" region, and "region except homologous domain" region, distribution patterns of the missense mutations causing SMEI ("pore"/"other homologous domain"/"region except homologous domain"; 22/11/9) and SMEB (13/2/3) did not differ ($p = 0.3142$), whereas those causing GEFS+ (4/8/2) and SMEI in the broad sense (SMEIBS; including both SMEI and SMEB) (32/13/12) did ($p = 0.0402$). Furthermore, the ratio of missense mutations in the pore regions to those in all four homologous domains (32/45, 71.1%) was higher for the SMEIBS group than for the GEFS+ group (4/12, 33.3%) ($p = 0.0220$), indicating that missense mutations that occur in "pore" regions more frequently are accompanied by the SMEI than the GEFS+ phenotype.

In the SMEIBS group patients, mean disease onset showed a tendency to earlier onset in those with mutations

in the "pore" region (n = 31; 5.81 ± 0.42 months ± SEM) than in those with mutations in the "insulating" region (n = 7; 7.29 ± 0.89 months) (p = 0.091, figure 2A).

Moreover, the ratio of SMEIBS patients with ataxia to those without it was higher in those patients with mutations in the "pore" (15/20, 75%) than in the "insulating" (1/6, 16.7%) regions (p = 0.018, figure 2B). There was no significant difference among groups in terms of the other clinical symptoms analyzed (sex and severity of mental retardation).

Interestingly, we identified an R946C mutation in the highly conserved DII S5-S6 linker region[12] (see figure 1, A and B) in both the SMEI and SMEB patients.

Discussion. This study was carried out to answer the question "Why do similar missense mutations in *SCN1A* cause two such different phenotypes (GEFS+/SMEI), although almost all the truncation mutations of *SCN1A* result in SMEI?"

The α1 subunit of sodium channel consists of four internally homologous domains, each containing six transmembrane segments (S1-S6). These four homologous domains are pseudosymmetrically arranged around a central pore whose structural constituents determine the selectivity and conductance properties of the channel. Especially, S5 and S6 segments and the S5-S6 linker line the permeation pathway, and it has been proved that these segments can solely consist of functional pore.[18] These segments are also considered to play important roles in ion selectivity (DEKA ring aligned in the sodium channel pore[19] and the surrounding sequences near DEKA ring[20,21]) and gating kinetics[22,23] that are crucial for generating the electromotive forces required for electrical signaling.

With regard to other ion channels, several pathogenic mutations in the pore regions of the channels have also been reported. Autosomal dominant nocturnal frontal lobe epilepsy (ADNFLE) is caused by mutations in the nicotinic acetylcholine receptor (nAChR) α4 and β2 subunit genes *CHRNA4* and *CHRNB2*, and all mutations causing ADNFLE lie within (or immediately adjacent to) M2, the putative pore-forming region of nAChR.[24] Several mutations causing benign familial neonatal convulsions also lie within the pore forming region of the potassium channel genes *KCNQ2* and *KCNQ3*,[25] including the ion selective filter region in the pore.[26]

As stated, missense mutations in the pore regions of *SCN1A* were associated with a more severe phenotype (SMEI phenotype, a complication of ataxia and tendency of early disease onset) than were mutations in other regions, although the power of analysis of SMEI/GEFS+ phenotype was rather low, possibly because of the small sample size of the GEFS+ group. The reason is not clear. What differences exist in the sodium channel dysfunctions produced by mutations in the pore regions and by those in other regions have yet to be clarified. However, several recent reports revealed that some *SCN1A* missense mutations bearing GEFS+ or SMEI/SMEB were associated with altered channel activation/inactivation, voltage dependency,[27,28] and markedly reduced inward sodium currents.[29] One of the probable explanations is that mutations in the pore regions may

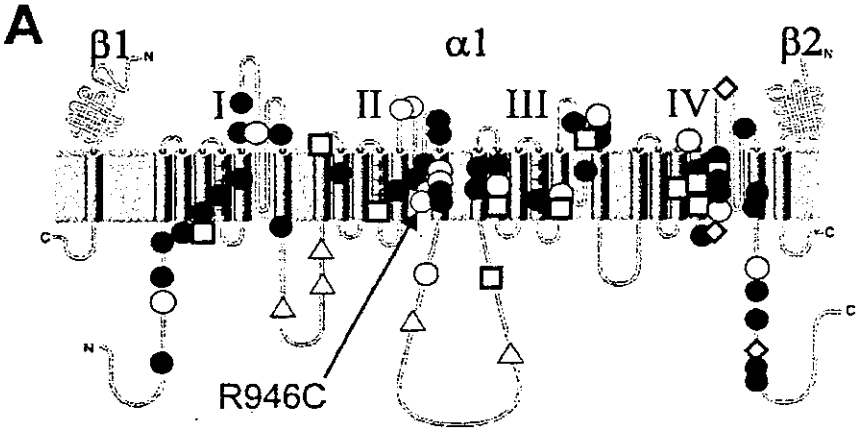

Figure 1. (A) Distribution of reported missense mutations in SCN1A.[2-9,11-15] *Solid circle: missense mutation identified in severe myoclonic epilepsy of infancy (SMEI) patients; open circle: mutation identified in borderline SMEI (SMEB); meshed circle: mutation identified both in SMEI and SMEB; open square: mutation identified in generalized epilepsy with febrile seizures plus (GEFS+); open diamond: mutation identified both in GEFS+ and SMEI/SMEB patients; open triangle: mutation identified in patients with idiopathic generalized epilepsy. R946C is indicated by the arrow. (B) Evolutionary conservation of arginine residue 946 (R946) and amino acid alignment near it. R946 and surrounding amino acid alignment are highly conserved among* SCN1A, SCN4A, *and* scn4a. *R946 in* SCN1A *is comparable to R756 in* SCN4A *and R750 in* scn4a *(enclosed by the dotted box).*

Table 2 Distribution patterns of missense mutations in GEFS+, SMEI, SMEB, and the total SMEI group

Segment	GEFS+	SMEI	SMEB	SMEIBS
S1	0	2	0	2
S1–S2 linker	1	0	0	0
S2	1	2	1‡	3
S2–S3 linker	1	1	0	1
S3	1	1	0	1
S3–S4 linker	0	0	1	1
S4*	3	3	0	3
S4–S5 linker	1§	2§	0	2
S5†	2¶	4¶	3	7
S5–S6 linker†	2§	12§	8§‖	17
S6†	0	6	2	8
Interdomain linker	1	1	1‡	2
N-terminal	0	3	1	4
C-terminal	1§	5	1	6§

* "Voltage sensor" region in *SCN1A*.
† "Pore" forming region in *SCN1A*.
‡ T808S/N1011S is counted both in S2 and in the interlinker domain.
§ P1668A and M1852T are counted in both GEFS+ and SMEI, and T1709I in both GEFS+ and SMEB.
¶ F1692S is counted only in SMEI, because the father of the patient with F1692S showed only simple FS.
‖ R931C, M934I, and R946C are counted both in SMEI and SMEB.

GEFS+ = generalized epilepsy with febrile seizures plus; SMEI = severe myoclonic epilepsy of infancy; SMEB = borderline SMEI; FS = febrile seizures.

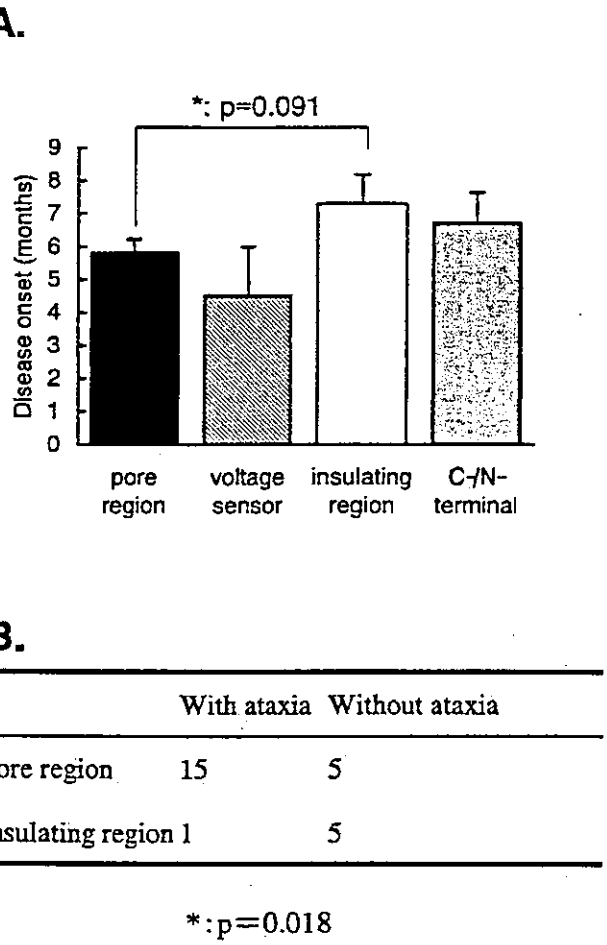

*Figure 2. Result of clinical data analysis. (A) Mean disease onset in the total severe myoclonic epilepsy of infancy (SMEI) group classified by mutation location. Pore region; mutations present in that region (S5, S6, or S5-S6 linker). Voltage sensor; mutations present in the voltage sensor region (S4). Insulating region; mutations in internal homologous regions other than the pore and voltage sensor regions. C-/N-terminal; mutations in the C- or N-terminal. * p = 0.091. (B) The number of subjects with/without ataxia in the total SMEI group divided according to the mutation location. With ataxia; number of SMEI patients with ataxia. Without ataxia; number of SMEI patients without ataxia. * p = 0.018.*

produce more severe channel dysfunction, including activation/inactivation dysfunction or abnormal voltage dependency, than those in other transmembrane regions. This may also affect the patients' phenotype, i.e., GEFS+ or SMEI.

Several other mechanisms are suggested as explaining why *SCN1A* missense mutations are found in both GEFS+ and SMEI. For example, not only the localization of *SCN1A* missense mutations but also the type of missense mutations, i.e., amino acid residue substitutions, may be important in determining disease severity.[15] This issue will be discussed in the near future when more cases are made available. On the other hand, different incidences of *SCN1A* mutation among SMEI patients[7,8,10-15] have been reported (33% to 100%), and these values are clearly higher than those of GEFS+ patients (about 10% or less).[30] In addition, families that have both SMEI and asymptomatic subjects who share a common mutation[8] were also reported. Those data suggest that other responsible or modifying genes are involved in the pathogenesis of GEFS+ or SMEI or both.[15]

Another possible mechanism, directly related to *SCN1A* missense mutations in the pore regions, is suggested by the mutation of R946C, reported previously by our group.[15]

Sodium channels have some highly conserved regions in their structure, i.e., the DII S5-S6 linker segment (see figure 1, A and B). Mutated *sca4a* (μ1) carrying R750C, comparable to R946C in human *SCN1A*, is reported to have abnormal ion selectivity (abnormal permeability to K^+ and NH_3^+) in expressed cultured cells.[21] Abnormal ion selectivity in the mutated channels would affect several ion concentration gradients and neuronal excitability, and it has been considered as one of the possible causes of neuromuscular channelopathies.[31] Although circumstantial, these findings suggest that abnormal ion selectivity in the mutated channels contributes to the SMEI phenotype of R946C. Similar mechanisms

also may be involved in the pathophysiology or the severe phenotype (i.e., the SMEI phenotype, ataxia, and tendency to earlier disease onset) of other mutations in the pore region.

Whereas we sought to analyze the localization of missense mutations in *SCN1A*, several additional factors should be involved in the pathogenesis of SMEI/GEFS+ (e.g., types of amino acid residue substitutions). Furthermore, the truncation mutations in *SCN1A* causing SMEI, of course, are also important. Many truncation (and several missense) mutations causing SMEI lie in the C terminus of *SCN1A*.[15] The C terminus in *SCN1A* would also be important in the pathogenesis of SMEI. Further clinical and neuroscientific studies are needed to clarify these issues.

References

1. Kaneko S, Okada M, Iwasa H, et al. Genetics of epilepsy: current status and perspectives. Neurosci Res 2002;44:11–30.
2. Escayg A, MacDonald BT, Meisler MH, et al. Mutations of *SCN1A*, encoding a neuronal sodium channel, in two families with GEFS+2. Nat Genet 2000;24:343–345.
3. Wallace RH, Scheffer IE, Barnett S, et al. Neuronal sodium-channel alpha1-subunit mutations in generalized epilepsy with febrile seizures plus. Am J Hum Genet 2001;68:859–865.
4. Escayg A, Heils A, MacDonald BT, et al. A novel *SCN1A* mutation associated with generalized epilepsy with febrile seizures plus—and prevalence of variants in patients with epilepsy. Am J Hum Genet 2001;68:866–873.
5. Sugawara T, Mazaki-Miyazaki E, Ito M, et al. $Na_v1.1$ mutations cause febrile seizures associated with afebrile partial seizures. Neurology 2001;57:703–705.
6. Abou-Khalil B, Ge Q, Desai R, et al. Partial and generalized epilepsy with febrile seizures plus and a novel *SCN1A* mutation. Neurology 2001;57:2265–2272.
7. Fujiwara T, Sugawara T, Mazaki-Miyazaki E, et al. Mutations of sodium channel alpha subunit type 1 (SCN1A) in intractable childhood epilepsies with frequent generalized tonic-clonic seizures. Brain 2003; 126:531–546.
8. Nabbout R, Gennaro E, Dalla Bernardina B, et al. Spectrum of *SCN1A* mutations in severe myoclonic epilepsy of infancy. Neurology 2003;60: 1961–1967.
9. Annesi G, Gambardella A, Carrideo S, et al. Two novel *SCN1A* missense mutations in generalized epilepsy with febrile seizure plus. Epilepsia 2003;44:1257–1258.
10. Claes L, Del-Favero J, Ceulemans B, Lagae L, Van Broeckhoven C, De Jonghe P. De novo mutations in the sodium-channel gene *SCN1A* cause severe myoclonic epilepsy of infancy. Am J Hum Genet 2001;68:1327–1332.
11. Sugawara T, Mazaki-Miyazaki E, Fukushima K, et al. Frequent mutations of SCN1A in severe myoclonic epilepsy of infancy. Neurology 2002;58:1122–1124.
12. Ohmori I, Ouchida M, Ohtsuka Y, Oka E, Shimizu K. Significant correlation of the SCN1A mutations and severe myoclonic epilepsy in infancy. Biochem Biophys Res Commun 2002;295:17–23.
13. Claes L, Ceulemans B, Audenaert D, et al. De novo *SCN1A* mutations are a major cause of severe myoclonic epilepsy of infancy. Hum Mutat 2003;21:615–621.
14. Fukuma G, Oguni H, Shirasaka Y, et al. Mutations of neuronal voltage-gated Na^+ channel a1 subunit gene *SCN1A* in core severe myoclonic epilepsy in infancy (SMEI) and in borderline SMEI (SMEB). Epilepsia 2004;45:140–148.
15. Wallace RH, Hodgson BL, Grinton BE, et al. Sodium channel α1-subunit mutations in severe myoclonic epilepsy of infancy and infantile spasms. Neurology 2003;61:765–769.
16. Ohmori I, Ohtsuka Y, Ouchida M, et al. Is phenotype difference in severe myoclonic epilepsy in infancy related to *SCN1A* mutations? Brain Dev 2003;25:488–493.
17. Commission on Classification and Terminology of the ILAE. Proposal for revised classification of epilepsies and epileptic syndromes. Epilepsia 1989;30:389–399.
18. Chen Z, Alcayaga C, Suarez-Isla BA, et al. A "minimal" sodium channel construct consisting of ligated S5-P-S6 segments forms a toxin-activatable Ionophore. J Biol Chem 2002;277:24653–24658.
19. Heinemann SH, Terlau H, Stuhmer W, Imoto K, Numa S. Calcium channel characteristics conferred on the sodium channel by single mutations. Nature 1992;356:441–443.
20. Tsushima RG, Li RA, Backx PH. Altered ionic selectivity of the sodium channel revealed by cysteine mutations within the pore. J Gen Physiol 1997;109:463–475.
21. Yamagishi T, Li RA, Hsu K, Marban E, Tomaselli GF. Molecular architecture of the voltage-dependent Na channel: functional evidence for alpha helices in the pore. J Gen Physiol 2001;118:171–182.
22. Vilin YY, Fujimoto E, Ruben PC. A single residue differentiates between human cardiac and skeletal muscle Na^+ channel slow inactivation. Biophys J 2001;80:2221–2230.
23. Hilber K, Sandtner W, Kudlacek O, et al. The selectivity filter of the voltage-gated sodium channel is involved in channel activation. J Biol Chem 2001;276:27831–27839.
24. Rodrigues-Pinguet N, Jia L, Li M, et al. Five ADNFLE mutations reduce the Ca^{2+} dependence of the mammalian $\alpha4\beta2$ acetylcholine response. J Physiol 2003;550:11–26.
25. Robbins J. KCNQ potassium channels: physiology, pathophysiology, and pharmacology. Pharmacol Ther 2001;90:1–19.
26. Hirose S, Zenri F, Akiyoshi H, et al. A novel mutation of *KCNQ3* (c. 925T–>C) in a Japanese family with benign familial neonatal convulsions. Ann Neurol 2000;47:822–826.
27. Spampanato J, Escayg A, Meisler MH, Goldin AL. Functional effects of two voltage-gated sodium channel mutations that cause generalized epilepsy with febrile seizures plus type 2. J Neurosci 2001;21:7481–7490.
28. Spampanato J, Escayg A, Meisler MH, Goldin AL. Generalized epilepsy with febrile seizures plus type 2 mutation W1204R alters voltage-dependent gating of $Na_v1.1$ sodium channels. Neuroscience 2003;116: 37–48.
29. Sugawara T, Tsurubuchi Y, Fujiwara T, et al. $Na_v1.1$ channels with mutations of severe myoclonic epilepsy in infancy display attenuated currents. Epilepsy Res 2003;54:201–207.
30. Sugawara T, Tsurubuchi Y, Agarwale KL, et al. A missense mutation of the Na^+ channel $\alpha2$ subunit gene *$Na_v1.2$* in a patient with febrile and afebrile seizures causes channel dysfunction. Proc Natl Acad Sci 2001; 98:6384–6389.
31. Noebels JL. Exploring new gene discoveries in idiopathic generalized epilepsy. Epilepsia 2003;44 suppl 2:16–21.

British Journal of Clinical Pharmacology DOI:10.1111/j.1365-2125.2004.02208.x

Effect of itraconazole on the pharmacokinetics and pharmacodynamics of a single oral dose of brotizolam

T. Osanai,[1] T. Ohkubo,[1] N. Yasui,[2] T. Kondo[2] & S. Kaneko[2]

[1]*Clinical Research Center, Hirosaki University Hospital, Hirosaki and* [2]*Department of Neuropsychiatry, Hirosaki University School of Medicine, Hirosaki University Hospital, Hirosaki, Japan*

Correspondence
Dr T. Ohkubo, Clinical Research Center, Hirosaki University Hospital, 53 Honchi, Hirosaki City, 036-8563 Japan.
Tel/Fax: +81 172 39 5295
E-mail: ok1231@cc.hirosaki-u.ac.jp

Keywords
brotizolam, CYP3A4, drug interaction, itraconazole, pharmacokinetics

Received
11 August 2003
Accepted
30 April 2004

Aims
To assess the effect of itraconazole, a potent inhibitor of cytochrome P450 (CYP)3A4, on the single oral dose pharmacokinetics and pharmacodynamics of brotizolam.

Methods
In this randomized, double-blind, cross-over trial 10 healthy male subjects received either itraconazole 200 mg or matched placebo once daily for 4 days. On day 4, a single 0.5 mg dose of brotizolam was administered orally. Plasma concentrations of brotizolam were followed up to 24 h, together with assessment of psychomotor function measured by the digit symbol substitution test (DSST), visual analogue scales and UKU side-effect rating scale.

Results
Itraconazole significantly ($P < 0.001$) decreased the apparent oral clearance (CL/F) (16.47 ± 4.3 *vs* 3.91 ± 2.1), increased the area under the concentration-time curves (AUC) from 0 h to 24 h (28.37 ± 10.8 *vs* 68.71 ± 24.1 ng ml h^{-1}), and prolonged the elimination half-life (4.56 ± 1.4 *vs* 23.27 ± 10.3 h) of brotizolam. The AUC(0,24 h) of the DSST ($P < 0.001$) and the item 'sleepiness' of UKU ($P < 0.05$) were significantly decreased.

Conclusions
Itraconazole increases plasma concentrations of brotizolam probably via its inhibitory effect on CYP3A4 brotizolam metabolism.

Introduction

Brotizolam, one of the triazolothienodiazepine derivatives, is widely used as a short acting hypnotic agent in Japan and Europe. Brotizolam is rapidly and completely absorbed after oral administration, with an elimination half-life in the range of 3–6 h [1]. Bioavailability of brotizolam is assumed to be around 65% based on calculating the ratio of the dose-normalized cumulative amount excreted in four subjects [2]. Brotizolam is metabolized almost completely into hydroxylated compounds identified as α-hydroxybrotizolam and 6-hydroxybrotizolam [3]. α-hydroxybrotizolam is almost as equi-effective as brotizolam but 6-hydroxybrotizolam has less activity than α-hydroxybrotizolam [4]. All hydroxy metabolites are almost completely conjugated to glucuronic acid and/or to sulfolic acid, which are rapidly excreted in urine [3, 4]. A recent paper reported that the brotizolam was metabolized to α-hydroxybrotizolam and 6-hydroxybrotizolam by CYP3A4 in human liver microsomes [5]. It is well known that triazolam and midazolam, which are benzodiazepines used as hypnotic agents, are metabolized by the CYP3A subfamily *in vitro* [6]. Furthermore, we reported that erythromycin, an inhibitor of CYP3A4, inhibits the metabolism of

alprazolam in healthy volunteers, which provided the first *in vivo* evidence for the involvement of CYP3A4 in the metabolic pathway of alprazolam [7]. The widely used azole antifungal agents ketoconazole and itraconazole are also potent inhibitors of CYP3A4 [8–10]. These antifungal agents strongly interact with orally ingested midazolam and triazolam, increasing the AUC values of these drugs by more than 10 fold [11, 12]. It is considered likely that brotizolam would interact with these antifungal agents but there are no *in vivo* data demonstrating this. In this study, we examined the effect of itraconazole on the pharmacokinetics and pharmacodynamics of brotizolam in healthy volunteers.

Methods

Subjects

The subjects were 10 healthy male volunteers. Their mean ± SD age was 33.7 ± 5.2 years and body weight 62.3 ± 4.6 kg. Their normal health status was confirmed by medical history, physical examination and haematology and blood chemistry tests. Five subjects were smokers (≥10 cigarettes day^{-1}), and the remaining five were non-smokers. None of the subjects used any concomitant medications. The study protocol was approved by the Ethics Committee of Hirosaki University Hospital, and each subject provided written informed consent to participate.

Protocol

The study was performed as a randomized, double-blind cross-over trial, with a washout period of 6 weeks between the two phases. The subjects took either itraconazole (200 mg) as a capsule formulation (Itrizole®, Janssen-Kyowa Co. Ltd, Tokyo, Japan) or matched placebo (as a capsule formulation with the same appearance and size as the itraconazole) once a day (between 11.30 and 12.30 h) for 4 days. On day 4, the subjects received a single oral 0.5 mg dose of brotizolam (Rendormin®, Japan Boehringer Ingelheim Co. Ltd. Tokyo, Japan) 1 h after the last dose of itraconazole or placebo. No food was allowed until 3 h after brotizolam dosing. The blood samples (10 ml each) were collected by venepuncture into heparinized tubes at 0, 0.5, 1, 1.5, 2, 3, 4, 6, 8, 10, 12 and 24 h after the brotizolam dosing. The blood samples were immediately centrifuged (1900 × *g*) at ambient temperature and the plasma layer was separated and stored at –40 °C until analysis.

Data analysis of pharmacodynamics

Psychomotor function status was evaluated at the same time points as blood samplings in both the control and itraconazole periods. This was done using the digit symbol substitution test (DSST), the number of digits correctly substituted with simple symbols, adapted from the Wechsler Adult Intelligence Scale in 3 min, the items 'thinking speed' of visual analogue scale (VAS) of mood and subjective states employed in the pharmacodynamic assessment study of chlordiazepoxide [13], and the item 'sleepiness' of the Udvalg for kliniske undersøgelser (UKU) side-effect rating scale [14]. The DSST variables were assessed by changed scores from baseline. The areas under the response-time curves (AUC) were determined by the trapezoidal rule for 0–24 h for each pharmacodynamic variable. Plots of effect-concentration data were made for mean values during each treatment. Effects-concentration data from DSST and UKU were inspected for the potential of pharmacodynamic modelling.

Drug assay

Plasma brotizolam concentrations were measured in duplicate by a high-performance liquid chromatography (HPLC) method developed in our laboratory [15]. Triazolam (5 ng) was added to the plasma samples (1 ml) as an internal standard, then the samples were diluted with 5 ml of 1 M sodium chloride and the solution was briefly mixed. The mixture was applied to a Sep-Pak C_{18} cartridge. The cartridge was then washed with 10 ml of water and 5 ml of 20% acetonitrile in water. The desired fraction was eluted with 5 ml of 40% acetonitrile in water. The eluent was evaporated to dryness at 60 °C. The residue was reconstituted in 100 µl of mobile phase. The samples were injected onto the HPLC. The lowest limit of detection was 0.5 ng ml^{-1}, and the coefficients of variation (both intra-assay and interassay) were less than 8.9%. Plasma itraconazole concentrations were measured using a solid phase extraction combined with the HPLC analysis method developed in our laboratory [16]. Bifonazole (30 ng) was added to the plasma samples (1 ml) as an internal standard, then the samples were diluted with 5 ml of 1 M sodium chloride and the solution briefly mixed. The mixture was applied to a Sep-Pak C_8 cartridge. The cartridge was then washed with 5 ml of water and 5 ml of 40% acetonitrile in water. The desired fraction was eluted with 5 ml of 80% acetonitrile in water. The eluent was evaporated to dryness at 60 °C. The residue was reconstituted in 60 µl of ethanol and 40 µl of mobile phase. The samples were injected onto the HPLC. The HPLC column used was a Grand Pack C_8-5 (MASIS Inc. Owani, Japan) with mobile phase consisting of 0.5% KH_2PO_4 (pH 4.5) : acetonitrile = 47 : 53. An ultraviolet detector was used to detect itraconazole and bifonazole. The

detection wavelength was set at 263 nm. The recovery of the extraction method was over 89.1% at several itraconazole concentrations. The lowest limit of detection was 5 ng ml^{-1} and the coefficients of variation (both intra-assay and interassay) were less than 6.9%.

Data analysis of pharmacokinetics

The elimination rate constant (λ_z) of brotizolam was estimated using linear regression analysis of the terminal log-linear concentration-time data, and the elimination half-life ($t^1_{/2}$) was calculated from $0.693/\lambda_z$. The area under the plasma concentration-time curve from 0 h to infinity (AUC(0,∞)) or total AUC, was calculated from AUC(0,24 h) + C_{24}/λ_z, where C_{24} is the plasma concentration of brotizolam at 24 h after the dosing. The apparent oral clearance (CL/*F*) was calculated from dose/total AUC. The peak plasma concentration (C_{max}) and the time to C_{max} (t_{max}) were determined graphically.

Statistical analysis

Results are expressed as mean values ± SD and the 95% confidence intervals for major differences between the phases. Pharmacokinetic and pharmacodynamic variables between the groups were compared by one-way ANOVA. ANOVA followed by Tukey's test was used for pharmacokinetic analysis based on log-transformed data, except for t_{max}, and ANOVA was also used for pharmacodynamic values. A significant difference was accepted when $P < 0.05$.

Results

The mean plasma brotizolam concentration-time data during treatment with placebo or itraconazole are shown in Figure 1. The mean (95% confidence interval) pharmacokinetics parameters are summarized in Table 1. When brotizolam was administered 1 h after the last dose of itraconazole, the oral clearance (CL/*F*) of brotizolam was reduced 0.23 fold (95% CI 0.14, 0.32; $P < 0.001$), the AUC(0,24 h) was increased 2.6 fold (95% CI 1.87, 3.39; $P < 0.002$) and the elimination $t_{1/2}$ increased 5.1 fold (95% CI 3.7, 6.5; $P < 0.001$) compared with control values. The t_{max} of brotizolam was also increased 4.2 fold (95% CI 2.4, 6.0; $P < 0.01$) during itraconazole treatment, but the C_{max} was not significantly higher. The second peak of brotizolam during itraconazole treatment probably originated from interindividual differences of measurement values. Plasma itraconazole concentration-time data on day 4 are shown in Figure 2. The mean maximum concentration of itraconazole was 324.2 ng ml^{-1}. There was a 5-fold interindividual variation in the C_{max} of itraconazole. The mean

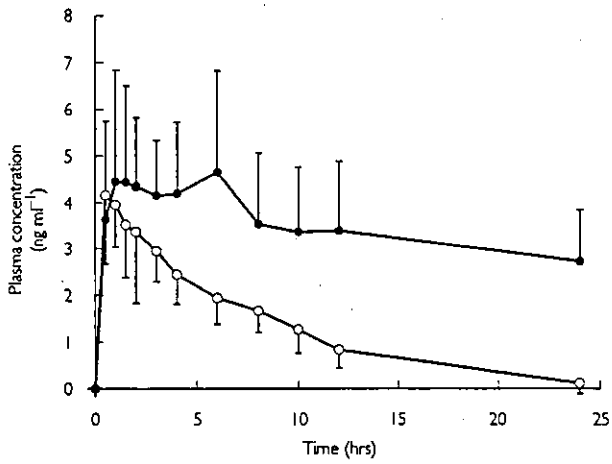

Figure 1
Plasma concentrations of brotizolam (mean ± SD) after an oral dose of 0.5 mg brotizolam following daily pretreatment with itraconazole 200 mg (●) or placebo (○) for 4 days in 10 healthy volunteers

Table 1
The pharmacokinetic variables of 0.5mg oral brotizolam (95% confidence interval, (95% CI)) in 10 subjects after pretreatment with placebo or 200mg itraconazole once daily for 4 days

Variable	Placebo (95% CI)	Itraconazole (95% CI)	Significance
C_{max} (ng ml^{-1})	4.82 (3.86, 5.75)	5.94 (4.42, 7.45)	NS
t_{max} (h)	0.75 (0.44, 1.05)	3.20 (1.86, 4.53)	$P < 0.05$
Elimination $t_{1/2}$ (h)	4.51 (3.67, 5.34)	23.27 (16.86, 29.65)	$P < 0.001$
CL/*F* (l h^{-1})	16.40 (13.70, 19.21)	3.91 (2.50, 5.31)	$P < 0.001$
AUC(0,24 h) (ng ml^{-1} h)	28.37 (21.64, 35.09)	68.71 (53.77, 83.64)	$P < 0.002$
AUC(0,∞) (ng ml^{-1} h)	33.10 (25.71, 40.40)	168.67 (110.20, 226.92)	$P < 0.001$

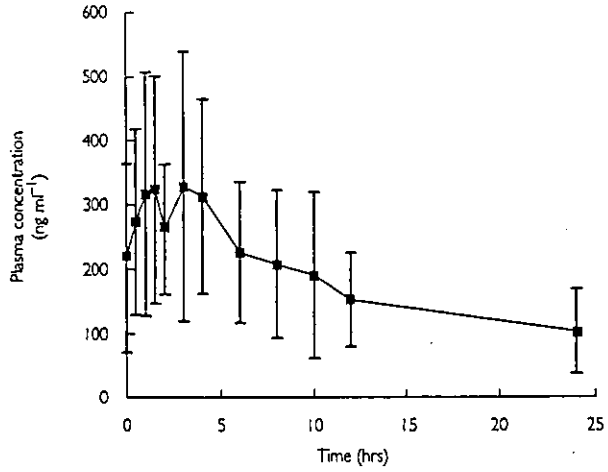

Figure 2
Plasma concentrations (mean ± SD) of itraconazole in 10 healthy volunteers on day 4

itraconazole concentration was over the 200 ng ml^{-1} at time 0 and over 100 ng l^{-1} after 24 h in the co-administration study. The mean AUCs (0,24 h) for each psychomotor function parameter are shown in Figure 3. The CNS-depressant effects of brotizolam, assessed by several psychomotor function tests, were observed for 24 h with recovery evident 24 h after drug administration. There were significant differences in the pharmacodynamic parameters (AUC(0,24 h)) of DSST (−3.8; 95% CI −7.41, 0.65; *vs* 9.1; 95% CI 5.06, 13.13, $P < 0.001$) and the item 'sleepness' of UKU (0.94; 95% CI 0.74, 1.14; *vs* 1.34; 95% CI 1.13, 1.54; $P < 0.05$) between the control and itraconazole arms of the study (Figure 3). No differences were found in AUC for any pharmacodynamic variables in VAS including the item of 'thinking' (−12.4; 95% CI −15.58, −9.36; *vs* −16.99; 95% CI −20.10, −13.89; $P = 0.05$) and 'Spacy' (−4.61; 95% CI −7.41, −1.81; *vs* −1.61; 95% CI −4.41, 1.19; $P = 0.123$) (Figure 3). A plot of mean change of DSST and UKU *vs* mean brotizolam plasma concentration shown in

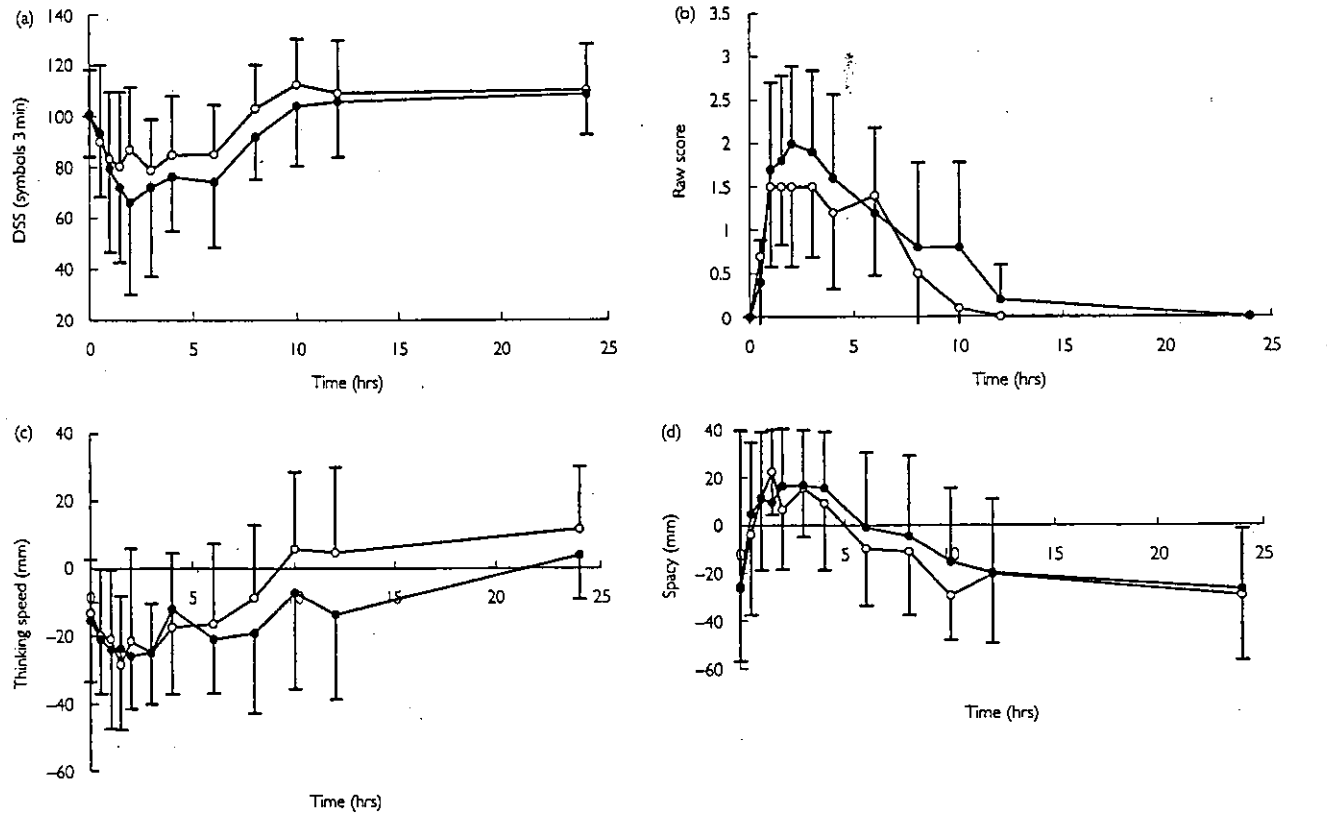

Figure 3
Results of the median score change in (a) digit symbol substitution test (DSST), (b) UKU side-effect rating scale (the item sleepiness), (c) VAS (thinking speed) and (d) VAS (Spacy) after an oral 0.5 mg dose of brotizolam following pretreatment with itraconazole (●) or placebo (○)

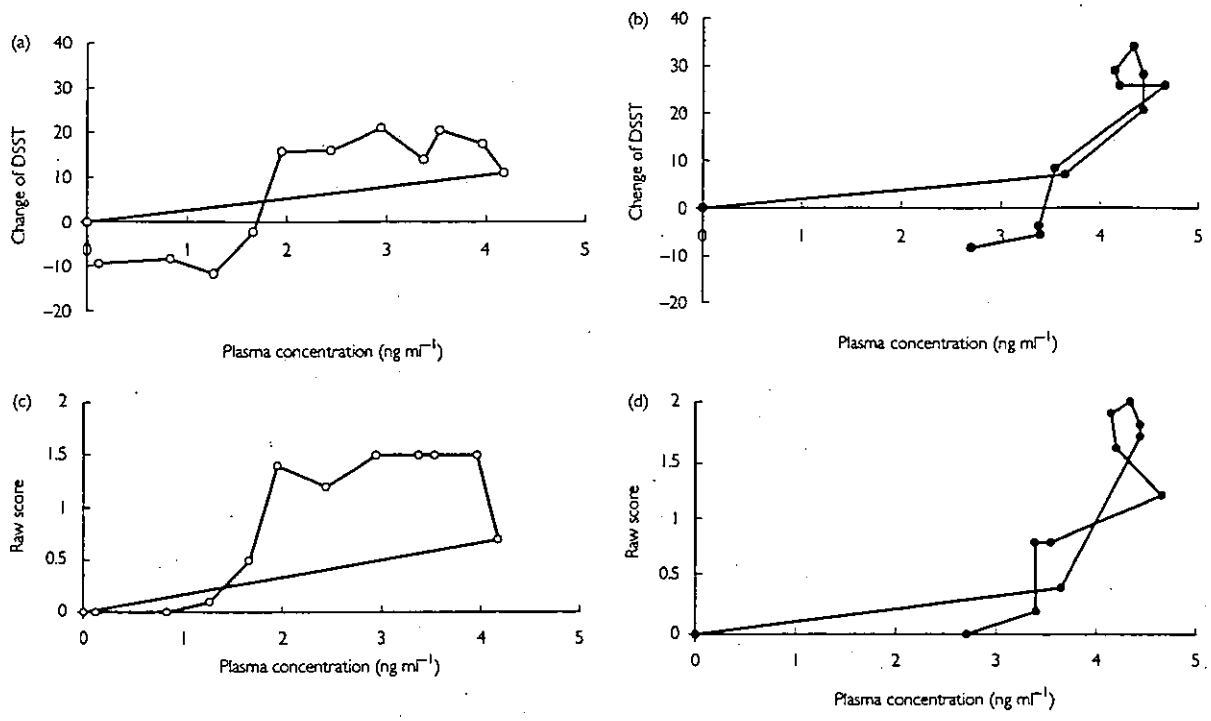

Figure 4
Plots of mean change in DSST in (a) control, (b) itraconazole and raw UKU score in (c) control, (d) itraconazole *vs* mean brotizolam plasma concentration

Figure 4 illustrates counter-clockwise hysteresis in both cases.

Discussion

Recent studies have uncovered many potentially hazardous interactions associated with the use of itraconazole, e.g. interactions with oral midazolam [11], triazolam [12] and zopiclone [17]. In the present study, itraconazole decreased CL/*F*, increased the AUC(0,24 h), and prolonged the elimination $t_{1/2}$ of brotizolam (Table 1). The results of the psychomotor tests were in good agreement with the pharmacokinetics findings (Figure 3). These findings provide further *in vivo* evidence of the involvement of CYP3A4 in brotizolam metabolism [5].

Previous studies have shown that itraconazole, in a dose of 200 mg day^{-1}, increased the mean AUC(0,∞) of triazolam by 27-fold [12], with significant linear correlation between the plasma concentration of itraconazole and AUC of triazolam [18]. Similarly, midazolam concentrations have increased 10-fold [11], supported by *in vitro* evidence of high inhibitory activity of itraconazole for CYP3A4 catalyzed hydroxylation of midazolam [19]. The concentrations of itraconazole in the present study were maintained at over 100 ng ml^{-1} until after 24 h, which appears to be high enough to inhibit the metabolism of brotizolam catalyzed by CYP3A4 *in vivo*.

Previous clinical studies suggested that itraconazole inhibited P-glycoprotein-mediated drug transportation [20, 21]. A recent *in vitro* study supported these results [22]. However, since two other benzodiazepines, midazolam and flunitrazepam, were not transported by P-glycoprotein *in vitro* [23, 24], it is unlikely that brotizolam is a clinically significant P-glycoprotein substrate.

Itraconazole altered not only the pharmacokinetics of brotizolam but also psychomotor function affected by brotizolam (Figure 3). The more depressed psychomotor function during itraconazole co-administration is probably explained by the elevated plasma concentrations of brotizolam. Physiological explanation for counter-clockwise hysteresis in pharmacodynamics *vs* plasma concentration plots (Figure 4) include delayed distribution to the effect site, delayed effect and sensitization or fatigue. Chronic tolerance also appeared to develop with itraconazole treatment. Previous papers have reported the development of tolerance to the pharmacodynamic effects during continuous and con-

stant plasma concentration of benzodiazepines [25, 26]. Therefore, the tolerance of brotizolam effects may be due to continuously high plasma concentrations of brotizolam by metabolic inhibition with itraconazole.

In conclusion, itraconazole significantly increases the plasma concentrations of brotizolam, probably through inhibition of CYP3A4, the major metabolic enzyme responsible for *in vivo* brotizolam elimination. Careful choice of dose of brotizolam is necessary in patients receiving itraconazole.

References

1 Jochemsen R, Hermans J, Van Boxtel CJ, Breimer DD. Pharmacokinetics of brotizolam in healthy subjects following intravenous and oral administration. Br J Clin Pharmacol 1983; 16: 285S–90S.

2 Bechtel WD, Van Wayjen RGA, Van Den Ende A. Blood level, excretion, and metabolite pattern of [^{14}C]-brotizolam in humans. Arzneimittelforschung 1986; 36: 578–86.

3 Bechtel WD. Pharmacokinetics and metabolism of brotizolam in human. Br J Clin Pharmacol 1983; 16: 279S–83S.

4 Danneberg P, Böke-Kuhn K, Bechtel WD, Lehr E. Pharmacological action of some known and possible metabolites of brotizolam. Arzneimittelforschung 1986; 36: 587–91.

5 Senda C, Kishimoto W, Sakai K, Nagakura A, Igarashi T. Identification of human cytochrome P450 isoforms involved in the metabolism of brotizolam. Xenobiotica 1997; 27: 913–22.

6 Kronbach T, Mathys D, Umeno M, Gonzales FJ, Meyer UA. Oxidation of midazolam and triazolam by human liver cytochrome P4503A4. Mol Pharmacol 1989; 36: 89–96.

7 Yasui N, Otani K, Kaneko S, Ohkubo T, Osanai T, Sugawara K, Chiba K, Ishizaki T. A kinetic and dynamic study of oral alprazolam with and without erythromycin in humans: in vivo evidence for the involvement of CYP3A4 in alprazolam metabolism. Clin Pharmacol Ther 1996; 59: 514–9.

8 Watkins PB. Noninvasive tests of CYP3A enzymes. Pharmacogenetics 1994; 4: 171–84.

9 Von Moltke LL, Greenblatt DJ, Harmatz JS, Duan SX, Harrel LM, Cotreau-Bibbo MM, Pritchard GA, Wraight CE, Shader RI. Triazolam biotransformation by human liver microzoms in vitro: effects of metabolic inhibitors and clinical confirmation of a predicted interaction with ketoconazole. J Pharmacol Exp Ther 1996; 276: 370–9.

10 Wilkinson GR. Cytochrome P4503A (CYP3A) metabolism: prediction of in vivo activity in humans. J Pharmacokinet Biopharm 1996; 24: 475–90.

11 Olkkola KT, Backman JT, Neuvonen PJ. Midazolam should be avoided in patients receiving the systemic antimycotics ketoconazole or itraconazole. Clin Pharmacol Ther 1994; 55: 481–5.

12 Varhe A, Olkkola KT, Neuvonen PJ. Oral triazolam is potentially hazardous to patients receiving systemic antimycotics ketoconazole or itraconazole. Clin Pharmacol Ther 1994; 56: 601–7.

13 Greenblatt DJ, Shader RI, Harmatz JS, Franke K, Koch-Weser J. Absorption rate, blood concentrations, and early response to oral chlordiazepoxide. Am J Psychiatry 1997; 134: 559–62.

14 Lingjaerde O, Ahlfors UG, Bech P, Dencher SJ, Elgen K. The UKU side effect rating scale: a new comprehensive rating scale for psychotropic drugs and a cross-sectional study of side effects in neuroleptic-treated patients. Acta Psychiatr Scand 1987; 76 (Suppl, 334): 11–100.

15 Osanai T, Ohkubo T. Development of high-performance liquid chromatographic method for determination of brotizolam on clinical pharmacokinetic study. Anal Lett 2003; 36: 3025–34.

16 Ohkubo T, Osanai T. Determination of itraconazole in human plasma by high-performance liquid chromatography with solid-phase extraction. Ann Clin Biochem 2004; in press.

17 Jalava K-M, Olkkola KT, Neuvonen PJ. Effect of itraconazole on the pharmacokinetics and pharmacodynamics of zopiclone. Eur J Clin Pharmacol 1996; 51: 331–4.

18 Neuvonen PJ, Varhe A, Olkkola KT. The effect of ingestion time interval on the interaction between itraconazole and triazolam. Clin Pharmacol Ther 1996; 60: 326–31.

19 Wang J-S, Wen X, Backman JT, Taavitsainen P, Neuvonen PJ, Kivistö KT. Midazolam α-hydroxylation by human liver microsomes *in vitro*: Inhibition by calcium channel blockers, itraconazole and ketoconazole. Pharmacol Toxicol 1999; 85: 157–61.

20 Jalava K-M, Partanen J, Neuvonen PJ. Itraconazole decreases renal clearance of digoxin. Ther Drug Monit 1997; 19: 609–13.

21 Lilija JJ, Backman JT, Laitila J, Luurila H, Neuvonen PJ. Itraconazole increases but grapefruit juice greatly decreases plasma concentrations of celiprolol. Clin Pharmacol Ther 2003; 73: 192–8.

22 Miyama T, Takanaga H, Matsuo H, Yamano K, Iga T, Naito M, Tsuruo T, Ishizuka H, Kawahara Y, Sawada Y. P-Glycoprotein-mediated transport of itraconazole across the blood–brain barrier. Antimicrob Agents Chemother 1998; 42: 1738–44.

23 Schinkel AH, Wagenaar E, Mol CAAM, van Deemter L. P-Glycoprotein in the blood–brain barrier of mice influence the brain penetration and pharmacological activity of many drugs. J Clin Invest 1996; 97: 2517–24.

24 Takano M, Hasegawa R, Fukuda T, Yumoto R, Nagai J, Murakami T. Interaction with p-glycoprotein and transport of erythromycin, midazolam and ketoconazole in Caco-2 cells. Eur J Pharmacol 1998; 358: 289–94.

25 Fleishaker JC, Phillips JP, Eller MG, Smith RB. Pharmacokinetics and pharmacodynamics of alprazolam following single and multiple oral doses of a sustained-release formulation. J Clin Pharmacol 1989; 29: 543–9.

26 Kroboth PD, Bertz RJ, Smith RB. Acute tolerance to triazolam during continuous and step infusions: Estimation of the effect offset rate constant. J Pharmacol Exp Ther 1993; 364: 1047–55.

Neuropsychopharmacology (2004) 29, 1901–1909

www.neuropsychopharmacology.org

A Missense Variation in Human *Casein Kinase I Epsilon* Gene that Induces Functional Alteration and Shows an Inverse Association with Circadian Rhythm Sleep Disorders

Atsuko Takano[1], Makoto Uchiyama[2], Naofumi Kajimura[3], Kazuo Mishima[4], Yuichi Inoue[5], Yuichi Kamei[6], Tsuyoshi Kitajima[7], Kayo Shibui[2], Masaaki Katoh[3], Tsuyoshi Watanabe[3], Yuki Hashimotodani[1], Toru Nakajima[8], Yuji Ozeki[9], Toru Hori[3], Naoto Yamada[9], Ryoichi Toyoshima[10], Norio Ozaki[7], Masako Okawa[9], Katsuya Nagai[1], Kiyohisa Takahashi[2,3,6], Yasushi Isojima[1], Toshio Yamauchi[10] and Takashi Ebisawa*[,10,11]

[1]Division of Protein Metabolism, Institute for Protein Research, Osaka University, Osaka, Japan; [2]Department of Psychophysiology, National Center of Neurology and Psychiatry (NCNP), Chiba, Japan; [3]Musashi Hospital, NCNP, Tokyo, Japan; [4]Department of Psychiatry, Akita University School of Medicine, Akita, Japan; [5]Department of Psychiatry, Juntendo University, School of Medicine, Tokyo, Japan; [6]Kohnodai Hospital, NCNP, Chiba, Japan; [7]Department of Psychiatry, Fujita Health University School of Medicine, Aichi, Japan; [8]Department of Neuropsychiatry, Kyorin University, School of Medicine, Tokyo, Japan; [9]Department of Psychiatry, Shiga University of Medical Science, Shiga, Japan; [10]Department of Neuropsychiatry, Saitama Medical School, Saitama, Japan; [11]Project Research Division in Research Center for Genomic Medicine, Saitama Medical School, Saitama, Japan

Recent studies have shown that functional variations in clock genes, which generate circadian rhythms through interactive positive/negative feedback loops, contribute to the development of circadian rhythm sleep disorders in humans. Another potential candidate for rhythm disorder susceptibility is casein kinase I epsilon (CKIε), which phosphorylates clock proteins and plays a pivotal role in the circadian clock. To determine whether variations in *CKIε* induce vulnerability to human circadian rhythm sleep disorders, such as delayed sleep phase syndrome (DSPS) and non-24-h sleep–wake syndrome (N-24), we analyzed all of the coding exons of the human *CKIε* gene. One of the variants identified encoded an amino-acid substitution S408N, eliminating one of the putative autophosphorylation sites in the carboxyl-terminal extension of CKIε. The N408 allele was less common in both DSPS ($p = 0.028$) and N-24 patients ($p = 0.035$) compared to controls. When DSPS and N-24 subjects were combined, based on an *a priori* prediction of a common mechanism underlying both DSPS and N-24, the inverse association between the N408 allele and rhythm disorders was highly significant ($p = 0.0067$, odds ratio = 0.42, 95% confidence interval: 0.22–0.79). *In vitro* kinase assay revealed that CKIε with the S408N variation was ~1.8-fold more active than wild-type CKIε. These results indicate that the N408 allele in *CKIε* plays a protective role in the development of DSPS and N-24 through alteration of the enzyme activity.

Neuropsychopharmacology (2004) **29,** 1901–1909, advance online publication, 9 June 2004; doi:10.1038/sj.npp.1300503

Keywords: casein kinase; polymorphism, single nucleotide; phosphorylation; biological clocks; case–control studies; risk factors

INTRODUCTION

In mammals, including humans, circadian cycles of approximately 24 h are observed in behavior and physiology, including cycles of sleep, hormone secretion, and core body temperature. The master circadian pacemaker is localized in the hypothalamic suprachiasmatic nucleus (SCN). Clock genes, *Per1/2/3*, *Cry1/2*, *Bmal1*, and *CLOCK* are expressed in the SCN and produce a nearly 24 h cycle through interacting positive/negative feedback loops (Harmer *et al*, 2001; Reppert and Weaver, 2002). BMAL1 and CLOCK proteins bind to E-box elements and activate transcription of *Per* and *Cry* genes. As the PERs and CRYs are translated, they enter the nucleus and inhibit BMAL1/CLOCK-driven transcription in the negative feedback loop. The circadian pacemaker is synchronized (entrained) to the 24 h day, primarily by the environmental light/dark cycle.

Certain human sleep disorders, designated circadian rhythm sleep disorders, are attributed to the disruption of the circadian timing system (Weitzman *et al*, 1981; Campbell *et al*, 1999; Wijnen *et al*, 2002). Patients with circadian

*Correspondence: Dr T Ebisawa, Department of Neuropsychiatry, Saitama Medical School, 38 Morohongo, Moroyama-cho, Iruma-gun, Saitama 350-0495, Japan, Tel: +81 492 76 1213, Fax: +81 492 76 1622, E-mail: tebisawa@saitama-med.ac.jp
Received 12 August 2003; revised 9 April 2004; accepted 12 May 2004
Online publication: 15 May 2004 at http://www.acnp.org/citations/Npp05150403365/default.pdf

rhythm sleep disorders, such as delayed sleep phase syndrome (DSPS), advanced sleep phase syndrome (ASPS), and non-24-h sleep–wake syndrome (N-24), fail to adjust their sleep/wake cycle to the daily schedule required for social life. Despite normal sleep architecture, sleep onset and offset are persistently delayed (DSPS) or advanced (ASPS) compared to the societal norm. N-24 patients suffer from daily delays of sleep onset and offset times, with the consequence of progressive cycling through the 24 h environmental day. The pathogenesis of DSPS and N-24 is not yet known, but several possible mechanisms have been proposed: reduced sensitivity of the oscillator to photic entrainment, a prolonged intrinsic period beyond the range of entrainment to 24 h day, and abnormal coupling of the sleep/wake cycle to the circadian rhythm (Weitzman *et al*, 1981; Campbell *et al*, 1999; Uchiyama *et al*, 2000). It is estimated that 0.13% (in Japan) (Yazaki *et al*, 1999), 0.17% (in Norway) (Schrader *et al*, 1993), and 0.7% (in USA) (Ando *et al*, 1995) of the general population suffer from DSPS, while the prevalence of N-24 is lower. Genetic factors reportedly confer predisposition to ASPS and DSPS (Ancoli-Israel *et al*, 2001; Jones *et al*, 1999; Reid *et al*, 2001).

Analysis of animals and humans with altered circadian rhythms demonstrated that casein kinase I epsilon (CKIε) (and presumably its most closely related homolog, CKIδ) plays a crucial role in regulating the circadian pacemaker (Eide and Virshup, 2001). CKIε (and CKI δ) phosphorylates PER proteins, leading to their destabilization and relocalization (Takano *et al*, 2000; Vielhaber *et al*, 2000; Keesler *et al*, 2000; Akashi *et al*, 2002; Camacho *et al*, 2001). CKIε/δ have long carboxyl-terminal (C-terminal) extensions, which can be autophosphorylated, with the consequence of autoinhibition of kinase activity (Graves and Roach, 1995; Cegielska *et al*, 1998). *Double-time* (*dbt*) gene, a Drosophila homolog of mammalian *CKIε*, was shown to alter or ablate circadian rhythm when functionally mutated (Price *et al*, 1998). In hamsters, a point mutation in *CKIε* that decreases kinase activity causes the semidominant short-period *tau* phenotype (Ralph and Menaker, 1988; Lowrey *et al*, 2000). A recent report showed that, in humans, familial ASPS can be induced by a *Per2* S662G mutation, which reduces CKIε-induced phosphorylation of the PER2 protein (Toh *et al*, 2001). We have reported that a *Per3* gene haplotype, in which one of the variations lies close to the CKIε target site and presumably alters PER3 protein phosphorylation, is significantly associated with DSPS (Ebisawa *et al*, 2001). These results suggest the possibility that human *CKIε* (h*CKIε*) gene may also be involved in susceptibility to circadian rhythm sleep disorders.

Accordingly, we set out to screen the complete coding region of the *CKIε* gene, as well as adjacent exon–intron boundaries for the presence of genetic variants in circadian rhythm sleep disorder patients and controls.

MATERIALS AND METHODS

Subjects

In all, 98 DSPS patients (60 males; 38 females; mean age: 27.1±9.1 years) and 39 N-24 patients (29 males; 10 females; mean age: 26.9±8.4 years) were recruited. Diagnosis was assigned by a trained psychiatrist according to the International Classification of Sleep Disorders (ICSD1990) criteria. All of the patients were unrelated, except for two sibling pairs, of which each consisted of a patient with DSPS and a patient with N-24. In a combined analysis of DSPS and N-24, two of the DSPS subjects with siblings of N-24 were excluded from the DSPS/N-24 group to avoid an increase in the Type I error rate. Neither of the sibling pairs carried the S408N variation. Another three patients with DSPS had relatives with probable DSPS, who were not involved in this study, and another patient with N-24 had a first-degree relative with severe insomnia. In all, 138 healthy subjects were recruited as controls (81 males; 57 females; mean age: 32.1±8.6 years). Control individuals were free from sleep disorders or psychoses. All of the study subjects were sighted. In total, 59 DSPS patients, 36 N-24 patients, and 107 control subjects of the study population were reported previously (Iwase *et al*, 2002), while the others were newly recruited for this study. In order to minimize the effect of the population stratification, which may cause false results, all of the study subjects were Japanese and recruited in mainland Japan. The controls were geographically matched to the patients. Written informed consent was obtained from the subjects. The protocol was approved by the ethics committee of Saitama Medical School and the participating institutes.

Blood samples were drawn by venipuncture and genomic DNAs were prepared from leukocytes using QIAamp DNA Blood Maxi Kit or QIAGEN Blood & Cell Culture DNA Midi Kit (QIAGEN, Hilden, Germany).

DNA Analysis

Polymerase chain reaction/single-strand conformation polymorphism (PCR-SSCP) analysis was used to screen for variations in all coding exons of the *CKIε* gene. Fluorescein-labelled primers to amplify each of the coding exons and adjacent exon–intron junctions were derived from the genomic structure determined by alignment of the cDNA and genomic sequence of hCKIε (AB024597 and AL020993, respectively) (Table 1). PCR was performed in a total volume of 50 μl containing 100 ng DNA, 0.5 μM of each primer, 1 × PCR buffer II, 0.2 mM dNTPs, 1.5 mM Mg^{2+}, and 1.25 U of AmpliTaq Gold DNA Polymerase. Conditions for PCR were preincubation at 95°C for 9 min to denature the DNA and to activate the polymerase, followed by 45 cycles at 95°C for 20 s, 63–68°C for 45 s, and 72°C for 1 min, with a subsequent final extension step at 72°C for 10 min.

SSCP electrophoresis was carried out on a denaturing gel in a DSQ-500S DNA sequencer (Shimadzu, Kyoto, Japan) basically as described (Ebisawa *et al*, 2001). Briefly, 1 μl of PCR products were mixed with 19 μl of formamide buffer (90% formamide, 5 mM EDTA, 10 mg/ml Blue dextran), heated at 80°C for 7 min, and 1.5 μl of the sample mixture was electrophoresed on a 0 or 5% glycerol SSCP Gel at 20°C, according to the manufacturer's protocol. Genomic DNAs in which variants were detected by SSCP were amplified using primers that encompass the SSCP-amplified region, and purified using QIAquick PCR Purification Kit (QIAGEN). Sequence reactions were performed on both strands using internal primers and the BigDye Terminator Cycle Sequencing Ready Reaction Kit (Applied Biosystems, Foster City, CA, USA) according to the protocol of the